

AFRL-ML-WP-TR-1998-4020

**SPLINE VARIATIONAL THEORY FOR
COMPOSITE BOLTED JOINTS**

E. Iarve and R. Y. Kim

University of Dayton Research Institute
300 College Park Avenue
Dayton, OH 45469-0168



JANUARY 1998

Interim Report for Period 15 September 1996 - 14 September 1997

Approved for public release; distribution unlimited.

19980820 098

MATERIALS AND MANUFACTURING DIRECTORATE
AIR FORCE RESEARCH LABORATORY
AIR FORCE MATERIEL COMMAND
WRIGHT-PATTERSON AIR FORCE BASE, OH 45433-7734

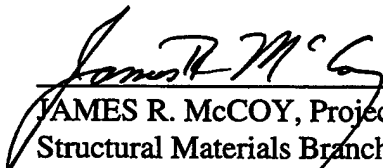
DTIC QUALITY INSPECTED 1

NOTICE


When government drawings, specifications, or other data are used for any purpose other than in connection with a definitely Government-related procurement, the United States Government incurs no responsibility or any obligation whatsoever. The fact that the government may have formulated or in any way supplied the said drawings, specifications, or other data, is not to be regarded by implication, or otherwise in any manner construed, as licensing the holder, or any other person or corporation; or as conveying any rights or permission to manufacture, use, or sell any patented invention that may be related thereto.

This report is releasable to the National Technical Information Service (NTIS). At NTIS, it will be available to the general public, including foreign nations.

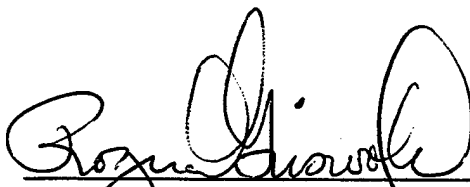
This technical report has been reviewed and is approved for publication.



JAMES R. McCOY, Project Engineer
Structural Materials Branch
Nonmetallic Materials Division



L. SCOTT THEIBERT, Chief
Structural Materials Branch
Nonmetallic Materials Division



ROGER D. GRISWOLD, Assistant Chief
Nonmetallic Materials Division
Materials and Manufacturing Directorate

If your address has changed, if you wish to be removed from our mailing list, or if the addressee is no longer employed by your organization, please notify AFRL/MLBC, Bldg 654, 2941 P St, Ste 1, Wright-Patterson AFB OH 45433-7750 to help us maintain a current mailing list.

Copies of this report should not be returned unless return is required by security considerations, contractual obligations, or notice on a specific document.

REPORT DOCUMENTATION PAGE			Form Approved OMB No. 0704-0188	
Public reporting burden for this collection of information is estimated to average 1 hour per response, including the time for reviewing instructions, searching existing data sources, gathering and maintaining the data needed, and completing and reviewing the collection of information. Send comments regarding this burden estimate or any other aspect of this collection of information, including suggestions for reducing this burden, to Washington Headquarters Services, Directorate for Information Operations and Reports, 1215 Jefferson Davis Highway, Suite 1204, Arlington, VA 22202-4302, and to the Office of Management and Budget, Paperwork Reduction Project (0704-0188), Washington, DC 20503.				
1. AGENCY USE ONLY (Leave blank)		2. REPORT DATE JANUARY 1998		3. REPORT TYPE AND DATES COVERED Interim Report - 9/15/96-9/14/97
4. TITLE AND SUBTITLE SPLINE VARIATIONAL THEORY FOR COMPOSITE BOLTED JOINTS			5. FUNDING NUMBERS F33615-95-D-5029 PE 62102F PR 4347 TA 34 WU 10	
6. AUTHOR(S) E. Iarve and R. Y. Kim				
7. PERFORMING ORGANIZATION NAME(S) AND ADDRESS(ES) University of Dayton Research Institute 300 College Park Avenue Dayton, OH 45469-0168			8. PERFORMING ORGANIZATION REPORT NUMBER UDR-TR-1998-00003	
9. SPONSORING/MONITORING AGENCY NAME(S) AND ADDRESS(ES) Materials and Manufacturing Directorate Air Force Research Laboratory Air Force Materiel Command Wright-Patterson AFB OH 45433-7734 POC: James R. McCoy, AFRL/MLBC, 937/255-9063			10. SPONSORING/MONITORING AGENCY REPORT NUMBER AFRL-ML-WP-TR-1998-4020	
11. SUPPLEMENTARY NOTES				
12a. DISTRIBUTION/AVAILABILITY STATEMENT Approved for public release; distribution unlimited.			12b. DISTRIBUTION CODE	
13. ABSTRACT (Maximum 200 words) A hybrid approximation model for predicting stresses and strains in open-hole composites was developed. This model is based on combined asymptotic and spline approximation stress functions and spline approximation displacement functions which provide accurate stress fields in the vicinity of the ply interface and the hole edge in a multilayered composite laminate. This hybrid model, using spline variational theory and Reissner's variational principle, provides directionally nonunique stress approximation critical for singular stress regions, combining it with flexibility of displacement approximation to analyze practical structures. Experimental studies of damage initiation and propagation in the open-hole laminates for three stacking sequences were performed. Theoretical strains obtained from the spline variational theory agree well with experimental strain measurements at low loadings prior to damage initiation.				
14. SUBJECT TERMS damage modeling, spline variational theory, open-hole composite, damage initiation, finite element, matrix cracks, composites, SVELT, graphite-epoxy, mechanical testing			15. NUMBER OF PAGES 52	
			16. PRICE CODE	
17. SECURITY CLASSIFICATION OF REPORT Unclassified	18. SECURITY CLASSIFICATION OF THIS PAGE Unclassified	19. SECURITY CLASSIFICATION OF ABSTRACT Unclassified	20. LIMITATION OF ABSTRACT SAR	

CONTENTS

Section		Page
1	COMBINED ASYMPTOTIC AND B-SPLINE-BASED APPROXIMATION FOR 3-D ANALYSIS OF COMPOSITE LAMINATES WITH OPEN HOLES	1
	1.1 Introduction	1
	1.2 Problem Statement	5
	1.3 Asymptotic Solution	6
	1.4 Variational Formulation	9
	1.5 Spline Approximation of Displacement Components	15
	1.6 Numerical Results	19
2	DAMAGE INITIATION AND PROGRESSION FOR BASIC LAMINATES WITH A HOLE	25
	2.1 Experiment	26
	2.2 Results and Discussion	29
	2.2.1 Analysis	29
	2.2.2 $[90_8]_T$ Laminate	29
	2.2.3 $[0_8]_T$ Laminate	31
	2.2.4 $[\pm 45]_{2S}$ Laminate	36
3	CONCLUSIONS/RECOMMENDATIONS	40
4	PUBLICATIONS/PRESENTATIONS	42
5	REFERENCES	43

FIGURES

Figure		Page
1	Laminated Plate and the Coordinate Systems, Respectively	5
2	Stress Intensity Factor for Different Superposition Region Sizes (a) and Different Subdivisions (b)	21
3	Shear Stress Calculated Using Total Displacement (a) and the Hybrid Expressions (b)	21
4	Angular Distribution of the Asymptotic Stress Functions	22
5	Transverse Normal Stress σ_{zz} - (a), $K(\theta)s_{zz}^a - s_{zz}^h$ - (b), and the Hybrid Approximation Stress $\bar{\sigma}_{zz}$ - (c)	24
6	Stress-Strain Curves from Gages e1-e5 for $[90_8]_T$ Laminate	30
7	Comparison of Strain Measurements with Axial Strain from SVELT	31
8	Radiographic Images of $[0_8]_T$ Specimen for Load Steps 1-4 and 8	32
9	Stress-Strain Curves for Gages e1-e6 for $[0_8]_T$ Laminate at Load Steps: (a) 183.9 MPa (26.67 ksi), (b) 229.8 MPa (33.33 ksi), (c) 270.7 MPa (39.26 ksi), (d) 332.0 MPa (48.15 ksi), (e) 510.7 MPa (74.07 ksi), and (f) 2119 MPa (307.3 ksi)	33
10	Experimental Strain Measurements from Gage e2 for Loadings 1-9	35
11	Comparison of Experimental and Theoretical Strains for $[0_8]_T$ Laminate	36
12	Radiographs of $[\pm 45]_{2S}$ Laminate for Stresses of (a) 114.9 MPa (16.66 ksi) and (b) 140.5 MPa (20.38 ksi)	36
13	Stress-Strain Curves for Gages e1-e5 for $[\pm 45]_{2S}$ Laminate at Load Steps: (a) 51.07 MPa (7.410 ksi), (b) 76.61 MPa (11.11 ksi), (c) 86.83 MPa (12.59 ksi), (d) 114.9 MPa (16.66 ksi), (e) 140.5 MPa (20.38 ksi), and (f) 158.3 MPa (22.96 ksi)	37
14	Experimental and Theoretical Strains for $[\pm 45]_{2S}$ Laminate	39

TABLES

Table		Page
1	Summary of Mechanical Properties for Basic Laminates	27

FOREWORD

This report was prepared by the University of Dayton Research Institute under Air Force Contract No. F33615-95-D-5029, Delivery Order No. 0004. The work was administered under the direction of the Nonmetallic Materials Division, Materials and Manufacturing Directorate, Air Force Research Laboratory, Air Force Materiel Command, with Dr. James R. McCoy (WL/MLBC) as Project Engineer.

This report was submitted in January 1998 and covers work conducted from 15 Sep 1996 through 14 Sep 1997.

EXECUTIVE SUMMARY

Ply-level models of laminated composites, according to which laminae are modeled as orthotropic plies, result in singular stress behavior in the vicinity of the ply interface and laminate edge. Numerical piecewise polynomial approximation-based approaches, such as displacement spline approximation, provide an accurate solution except in the vicinity of the singularity. A hybrid approximation, based on combined asymptotic and spline approximation stress functions and spline approximation displacement functions, was developed to provide accurate stress fields in the vicinity of the ply interface and the hole edge in a multilayered composite laminate. The singular term of the asymptotic analysis was used in hybrid stress functions. This term dominates the solution in the limit of zero distance from the singularity; however, the corresponding stress functions will not satisfy the three-dimensional equilibrium equations in any finite domain enclosing the singular point. Reissner's variational principle was applied and a procedure to determine the multiplicative factor of the singular term developed. A convergence study for a $[45/-45]_s$ laminate containing an open hole is presented. It was shown that the coarsest possible subdivision into one sublayer per ply provides converged values for the multiplicative factor of the singular term. The convergence was checked by comparison with results obtained with eight times more degrees of freedom. Converged interlaminar stresses including the singular point were obtained with two sublayers per ply thickness. The conventional approach based on displacement spline approximation required six sublayers through the thickness to obtain the multiplicative factor of the singular term at select circumferential locations. The combined asymptotic-spline approximation solution greatly increases the number of plies in the

laminate for which accurate interlaminar stresses can be obtained, by allowing coarser subdivisions.

The initiation and progression of damage for simple composite laminates with open holes under tension loading was recorded, and observations were correlated with results from experimental measurements from two-dimensional elasticity theory and from three-dimensional spline variational theory. During an incremental series of monotonic loadings, strain measurements were taken in close proximity to the hole boundary, while radiographic images were captured following each loading increment. This information provided a direct comparison between the state of damage and the state of strain. Three laminate stacking sequences were considered: $[0_8]_T$, $[90_8]_T$, and $[\pm 45]_{2S}$. As expected, the initiation of damage and laminate fracture occurred almost simultaneously for the $[90_8]_T$ laminate. Transverse cracking occurred prior to specimen failure for the $[0_8]_T$ and $[\pm 45]_{2S}$ laminates and is evident in the measured strain behavior. Overall, theoretical strains obtained from the spline variational theory agree well with experimental strain measurements at low loadings prior to damage initiation.

1. COMBINED ASYMPTOTIC AND B-SPLINE-BASED APPROXIMATION FOR 3-D ANALYSIS OF COMPOSITE LAMINATES WITH OPEN HOLES

1.1 Introduction

Significant practical interest represents development of methods for efficient stress analysis of composite structures containing curvilinear edges such as cutouts, etc. Ply level models of laminated composites, according to which lamina is modeled as an orthotropic ply, result in singular stress behavior in the vicinity of the ply interface and laminate edge. This report deals with three-dimensional stress analysis in the presence of singular stress concentrations and focuses on representing the stress field by using a superposition of the asymptotic solution and polynomial spline approximation.

Important experience was accumulated due to a large effort devoted to the solution of straight free-edge problems. A hybrid approximation, based on assumed in-plane stresses and the out-of-plane stresses defined to satisfy the equilibrium equations, was proposed by Pagano [1,2]. Reissner's variational principle was employed. Also, not including the precise singular stress terms, highly accurate stress predictions for various laminates were demonstrated. Wang and Choi [3,4] constructed an infinite series exact general solution for the same problem based on Lekhnitskii's complex variable stress function. The singular stress term was precisely determined. A polynomial particular solution was added to satisfy the axial loading condition. Determination of the unknown multiplicative factors in the homogeneous solution, including the multiplicative factor of the singular term, was accomplished by the boundary collocation method. The results were shown to converge for the number of Eigen functions of homogeneous solution equal to 30. A hybrid finite-element formulation (Tong, *et al.* [5]) based on this solution was developed by Wang and Yuan [6].

Folias [7] and Wang & Lu [8] considered stresses in laminated composites at the interface and open-hole edge. They showed that the zero's order term of asymptotic expansion of the three-dimensional elasticity equations upon parameter $\lambda=h/D$ (ply thickness/hole diameter) yields a plain strain elasticity problem. Thus, the singular stress term at the ply interface and curvilinear edge is the same as that for the straight edge provided the ply orientations are the same relative to the tangential to the curved edge. However, extending these results to obtain a full-field solution in the manner it was performed in two-dimensional cases is not trivial. The critical difference is that the analytically obtained Eigen functions of the asymptotic plain strain problem do not satisfy the original three-dimensional equations in any finite volume. Thus, no exact homogeneous solution is constructed to this point in a finite volume surrounding the intersection of the hole edge and orthotropic ply interface. It should be noted that the impressive convergence advantages of the hybrid singular finite element formulation were demonstrated [5,6] for problems where the assumed stress functions in relatively large singular elements actually provided the exact elasticity solutions over the entire element. An assumed displacement-based finite-element formulation, combining the asymptotic and polynomial approximation, was built by Wang and Lu [8] and the stress intensity factor for a $\pm 45^\circ$ laminate obtained as a function of the circumferential coordinate. Conciseness of this report, however, would not allow one to comment on the rate of convergence. It was noted that the asymptotic solution is included only over a small region near the free edge of the cutout.

Iarve [9] developed a B-spline-based displacement approximation three-dimensional solution for multilayered composite laminates containing open holes. It was also shown that a plane strain problem identical to the one obtained asymptotically in References [7] and [8] follows from the three-dimensional formulation by truncating the spatial derivatives in the

circumferential direction. The numerically obtained stress distributions near the hole edge were compared to the stresses given by the singular term of the asymptotic solution. At the singularity the polynomial spline approximation did not capture directional nonuniqueness of singular stress functions and resulted in interfacial traction discontinuity. However, it was observed that the singular term of the asymptotic solution with the appropriate coefficient matched the full-field spline approximation-based solution, with accuracy to additives-functions of the circumferential coordinate inside a region of up to one-half ply thickness from the singular point (except for the very vicinity of the singular point). The surprisingly large area of agreement suggests superimposing the singular term and the polynomial approximation, for accurate stress representation in the singular region.

Morley [10,11] pioneered the idea of superposition of the analytical and finite-element solution in problems with local field irregularity. The approach is based on the Rayleigh-Ritz method where polynomial displacement approximation is enriched through the entire domain by analytical solution minus its finite element projection. The analytical solution must be a particular solution of the problem. The finite-element projection is obtained by finite-element solution under the boundary conditions generated by the analytical solution with unit multiplicative factor. For sufficiently fine meshes the analytical solution and its projection will differ only in the vicinity of the singular point. The scaling factor, which is the coefficient of the additional terms used for enrichment of the finite element basis, is obtained through a variational procedure. Yamamoto and Tokuda [12] applied this method to crack stress intensity factor determination. They used the boundary collocation method to obtain the multiplicative factor of the terms containing analytical solutions.

For the curvilinear edge singularities considered in this report, no analytical solution in finite domain near the singularity is known. The asymptotic solution obtained in [7-9] is a plane strain solution in nature and cannot be used directly in the approach described in [10-12]. It should be mentioned that Yamamoto and Sumi [13] considered an axisymmetric problem of a twisted round isotropic bar with a circumferential crack. The asymptotic solution which was used as the basis for analytical solution near the crack tip was also a plane strain solution which doesn't satisfy the axisymmetric equilibrium equations. However, for the round isotropic bar problem, which was reduced to a single unknown function (the circumferential displacement component), the author found a higher-order term which was added to the asymptotic solution to satisfy the equilibrium equations. However, in a general orthotropic case, these complementary terms are not obvious and have not been reported in the literature.

This report extends the superposition approach to problems where no analytical solutions in the finite domain are known. The fact that the singular terms of the asymptotic solution result from the three-dimensional problem by truncating the spatial derivatives in the circumferential direction [9] will be used to construct a hybrid stress approximation. On the other hand, the corresponding asymptotic displacement functions should be avoided in the displacement approximation because the calculation of their derivatives in the circumferential direction, required in the variational formulation, is only numerically possible and undesirable. Thus, the approximation of stresses and displacements in this report will be independent, requiring Reissner's variational principle to be utilized.

1.2 Problem Statement

Consider a rectangular n -layer orthotropic plate with length L in the x -direction, width A in the y -direction and thickness H . Individual ply thickness is $h_s = z^{(s)} - z^{(s-1)}$, where $z = z^{(s)}$ and $z = z^{(s-1)}$ are upper and lower surfaces of the ply. The origin of the x, y, z coordinate system is in the lower left corner of the plate, as shown in Figure 1. Uniaxial loading is applied via displacement boundary conditions:

$$\begin{aligned} -u_x(0, y, z) &= u_x(L, y, z) = u_0, \\ u_y(0, y, z) &= u_y(L, y, z) = 0, \\ u_z(0, y, z) &= u_z(L, y, z) = 0, \end{aligned} \quad (1)$$

A circular opening of diameter D with the center in x_c, y_c is considered. The edge of the opening is part of the traction loading boundary ∂V_t , so that

$$\sigma_{ij} n_j = T_i, x_i \in \partial V_t$$

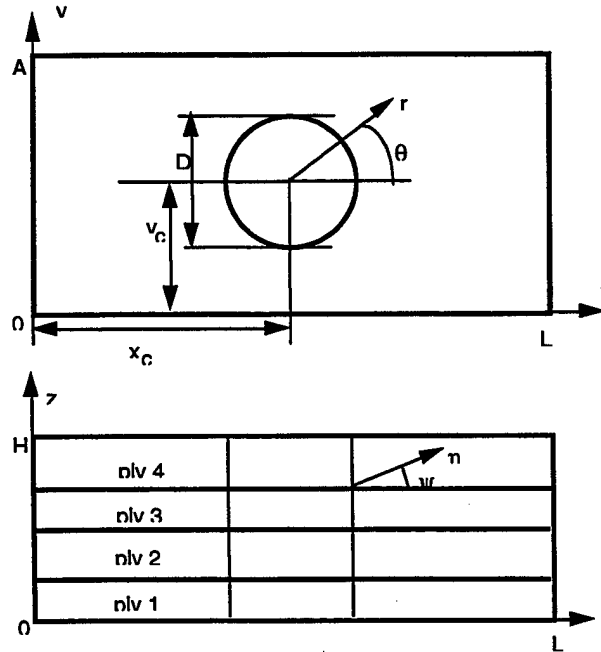


Figure 1. Laminated Plate and the Coordinate Systems, respectively.

where tractions T_i are prescribed. Indices $i,j=1,2,3$ correspond to directions x,y,z , respectively.

The lateral sides $y=0,A$ and the facial surfaces $z=0,H$ also belong to ∂V_i . A cylindrical

coordinate system r, θ, z with the origin in $x_c, y_c, 0$ is introduced and

$$x = r \cos \theta + x_c, y = r \sin \theta + y_c, z = z$$

The asymptotic solution in the vicinity of the hole edge and ply interface will be described next since it is essential for construction of the hybrid approximation.

1.3 Asymptotic Solution

A local coordinate system η, ψ is introduced in the r, z plane at the interface between p and $p+1$ plies in arbitrary radial cross-section $\theta=\text{const}$ as follows

$$r = \frac{D}{2} + H_p \eta \cos \psi, z = z^{(p)} + H_p \eta \sin \psi,$$

where $H_p = h_p + h_{p+1}$. For an arbitrary function F :

$$\begin{aligned} \frac{\partial F}{\partial r} &= \frac{1}{H_p} \Lambda_t F, \quad \frac{\partial F}{\partial z} = \frac{1}{H_p} \Lambda_n F, \\ \Lambda_t &= \frac{\partial F}{\partial \eta} \cos \psi - \frac{1}{\eta} \frac{\partial F}{\partial \psi} \sin \psi, \\ \Lambda_n &= \frac{\partial F}{\partial \eta} \sin \psi + \frac{1}{\eta} \frac{\partial F}{\partial \psi} \cos \psi, \end{aligned} \quad (2)$$

Establishing an asymptotic expansion parameter $\eta_0 = \max(\eta)$, one obtains that

$$\begin{aligned} \frac{\partial F}{\partial x} &= \frac{1}{H\eta_0} \cos \theta \Lambda_t F - \frac{1}{r} \sin \theta \frac{\partial F}{\partial \theta}, \\ \frac{\partial F}{\partial y} &= \frac{1}{H\eta_0} \sin \theta \Lambda_t F + \frac{1}{r} \cos \theta \frac{\partial F}{\partial \theta}, \\ \frac{\partial F}{\partial z} &= \frac{1}{H\eta_0} \Lambda_n F \end{aligned}$$

where η is replaced by η/η_0 in equation (2). Thus, for small η_0 the expressions for derivatives are truncated by keeping only first terms for the in-plane derivatives:

$$\begin{aligned}\frac{\partial F}{\partial x} &\equiv \frac{1}{H} \cos \theta \Lambda_t F \\ \frac{\partial F}{\partial y} &\equiv \frac{1}{H} \sin \theta \Lambda_t F \\ \frac{\partial F}{\partial z} &= \frac{1}{H} \Lambda_n F\end{aligned}\quad (3)$$

The parameter η_0 will be omitted elsewhere and assumed to be included in η . Under these assumptions the Lamé equations will simplify:

$$(\mathbf{A}\Lambda_t\Lambda_t + \mathbf{B}\Lambda_n\Lambda_t + \mathbf{C}\Lambda_n\Lambda_n) \begin{bmatrix} u_x \\ u_y \\ u_z \end{bmatrix} = 0,$$

where 3 by 3 matrices $\mathbf{A}, \mathbf{B}, \mathbf{C}$ were given in Larve [9] and depend upon material properties and θ .

The solution of these equations can be found in the form

$$u_i^a = \eta^\lambda \sum_{k=1}^6 \gamma_k d_{ki} (\sin \psi + \mu_k \cos \psi)^\lambda, \quad (4)$$

where

$$\det[\mathbf{A}\mu_k^2 + \mathbf{B}\mu_k + \mathbf{C}] = 0$$

and

$$[\mathbf{A}\mu_k^2 + \mathbf{B}\mu_k + \mathbf{C}] \begin{bmatrix} d_{k1} \\ d_{k2} \\ d_{k3} \end{bmatrix} = 0$$

The strains are calculated from displacements (4) by using truncated derivatives (3), and the stresses are obtained by using Hooke's law in the form

$$s_{ij}^a = \lambda \eta^{\lambda-1} \sum_{k=1}^6 \gamma_k c_{ij}^k (\sin \psi + \mu_k \cos \psi)^{\lambda-1} \quad (5)$$

The stresses are denoted s_{ij}^a to emphasize that functions (5) satisfy only the asymptotically-derived truncated equilibrium equations and compatibility equations. Coefficients γ_k are obtained to satisfy the traction-free conditions at the hole edge:

for $\psi = \pi/2$ ($p+1$ -th ply) and $\psi = -\pi/2$ (p -th ply)

$$s_{rr} = s_{r\theta} = s_{rz} = 0,$$

and the continuity conditions at the interface $\psi=0$:

$$\begin{aligned} u_i^{(p)} &= u_i^{(p+1)}, \\ s_{zz}^{(p)} &= s_{zz}^{(p+1)}, s_{zr}^{(p)} = s_{zr}^{(p+1)}, s_{z\theta}^{(p)} = s_{z\theta}^{(p+1)}. \end{aligned}$$

Nontrivial solutions of the problem exist for discrete λ only. The displacements (4) and stresses (5) are defined with accuracy to an arbitrary multiplicative factor. The multiplicative factor will be denoted as $K(\theta)$ and

$$u_i = K(\theta) u_i^a, \quad s_{ij} = K(\theta) s_{ij}^a$$

will also satisfy the truncated equilibrium equations and the boundary conditions. We shall be interested only in the solutions when $0 \leq \text{Re}(\lambda) < 1$. These terms provide unbounded stress functions which dominate the solution for small η . Equations (4) and (5) are normalized⁸ so that

$$K(\theta) = \lim_{\eta \rightarrow 0} (H_p \eta)^{1-\lambda} s_{zz}(\eta, 0, \theta).$$

1.4 Variational Formulation

A three-dimensional linear displacement approximation through the plate is written as

$$u_i = u_{im}^t \chi_i^m(x_i) \quad (6)$$

where $\chi_i^m(x_i)$ are sets of m basis functions, in general not identical for $i=1,2,3$. The total set of coefficients u_{im}^t consists of unknown coefficients u_{im} and fixed coefficients u_{im}^0 , so that u_i are kinematically admissible, i.e., satisfy (1) for arbitrary u_{im} . Summation is assumed upon repeated indices m . The nature of the functions $\chi_i^m(x_i)$ is not specified at this point. They may, in fact, include functions (4). We assume that $\chi_i^m(x_i)$ are continuous. The total displacement (6) is a superposition of two parts u_i^d and u_i^h . It is important to note that neither of these terms has to satisfy boundary conditions (1), only their superposition does. The stresses generated by the displacements u_i^d are calculated through Hooke's law, whereas the stresses generated by u_i^h are assumed as follows:

$$\bar{\sigma}_{ij}^h = \sum_{p=1}^{N-1} K_p(\theta) s_{ij}^{a,p} - s_{ij}^h + \sigma_{ij}^h,$$

where the bar sign is used to designate assumed stresses and

$$\sigma_{ij}^h = C_{ijkl}^{(p)} u_{(k,l)}^h,$$

$$s_{ij}^h = C_{ijkl}^{(p)} u_{(\bar{k},\bar{l})}^h,$$

The stiffness properties $C_{ijkl}^{(p)}$ are constant through the ply and considered as piecewise constant functions of z in the laminate. The notation

$$u_{(k,l)} = \frac{1}{2}(u_{k,l} + u_{l,k}), u_{(\bar{k},\bar{l})} = \frac{1}{2}(u_{\bar{k},\bar{l}} + u_{\bar{l},\bar{k}})$$

is used for conciseness, and the barred derivatives are calculated according to truncated expressions (3). Functions $s_{ij}^{a,p}$ are calculated using Equation (5) for the interface between plies $p, p+1$, and $K_p(\theta)$ are unknown functions. Since $u_i = u_i^h + u_i^d$ we shall choose u_i^h and u_i [Equation (1)] as independent functions. The combined hybrid stress approximation in the plate can be written:

$$\bar{\sigma}_{ij} = \sigma_{ij} - s_{ij}^h + \sum_{p=1}^{N-1} K_p(\theta) s_{ij}^{a,p}, \quad (7)$$

where

$$\sigma_{ij} = C_{ijkl}^{(p)} u_{(k,l)}.$$

Practically, the approximation (7) offers advantages only in the vicinity of the hole edge. We shall confine it to a region Γ , which is bounded by the hole surface, the upper and lower facial plate surfaces, and a vertical boundary $\partial\Gamma_v$ sufficiently far from the hole edge. Beyond this region it is assumed that

$$\bar{\sigma}_{ij} = \sigma_{ij}, x_i \in V - \Gamma.$$

The fact that the hybrid displacement portion is discontinuous $\partial\Gamma_v$ (it is zero outside Γ) does not imply discontinuity of the total displacement which is still given by (1). What is important is the stress continuity at $\partial\Gamma_v$. It will take place if

$$\sum_{p=1}^{N-1} K_p(\theta) s_{ij}^{a,p} - s_{ij}^h = 0, x_i \in \partial\Gamma_v$$

This condition will be shown to be satisfied if $\partial\Gamma_v$ is sufficiently far from the hole edge.

Reissner's variational principle $\delta R = 0$ is employed. Functional R :

$$R = \iiint_V (\Phi(\bar{\sigma}_{ij}) - \bar{\sigma}_{ij} u_{(i,j)}) dv + \iint_{\partial V_t} T_i u_i ds \quad (8)$$

is independently varied upon functions $\bar{\sigma}_{ij}$ and kinematically admissible u_i . Traction T_i are prescribed over the boundary ∂V_t and

$$\Phi(\sigma_{ij}) = \frac{1}{2} [C_{ijkl}^{(p)}] \sigma_{ij} \sigma_{kl}.$$

Substituting Equation (6) and (7) into (8), one obtains:

$$\begin{aligned} R = & \iiint_V \mathcal{Q} \left(\sum_{p=1}^{N-1} K_p(\theta) s_{ij}^{a,p}, u_{(i,j)}^h \right) dv \\ & - \iiint_V W(u_{(i,j)}) dv \\ & + \iint_{\partial V_t} T_i u_i ds. \end{aligned}$$

where

$$\begin{aligned} \mathcal{Q} = & \Phi \left(\sum_{p=1}^{N-1} K(\theta) s_{ij}^{a,p} \right) - \left(\sum_{p=1}^{N-1} K(\theta) s_{ij}^{a,p} \right) u_{(i,j)}^h \\ & + W(u_{(i,j)}^h), \end{aligned}$$

and

$$W(\epsilon_{ij}) = \frac{1}{2} C_{ijkl}^{(p)} \epsilon_{ij} \epsilon_{kl}.$$

Variation of R upon u_i^h , $K_p(\theta)$ and u_i , yields:

$$\begin{aligned}
\delta R = & - \iiint_V s_{ij,j}^h \delta u_i^h + \sum_{p=1}^{N-1} \iint_{z=z(p)} [s_{ij,n_j}^h] \delta u_i^h - \iint_{\partial V_t} \left(\sum_{p=1}^{N-1} K_p(\theta) s_{ij}^{a,p} - s_{ij}^h \right) n_j \delta u_i^h \\
& + \iiint_V \left(\Phi \left(\sum_{p=1}^{N-1} K_p(\theta) s_{ij}^{a,p}, s_{ij}^{a,m} \right) - s_{ij}^{a,m} u_{(i,j)}^h \right) \delta K_m(\theta) \\
& + \iiint_V \sigma_{ij,j} \delta u_i + \iint_{\partial V_t} (T_i - \sigma_{ij,n_j}) \delta u_i - \sum_{p=1}^{N-1} \iint_{z=z(p)} [\sigma_{ij,n_j}] \delta u_i
\end{aligned} \tag{9}$$

where

$$\Phi(\sigma_{ij}, \sigma_{ij}^*) = C_{ijkl}^{-1} \sigma_{ij} \sigma_{kl}^*.$$

It was taken into account that

$$s_{ij,j}^{a,p} = 0, \left[s_{ij,n_j}^{a,p} \right]_{z=z(p)} = 0.$$

The exact solution turns all integrands in (9) equal to zero. The equations obtained by varying u_i^h and $K_p(\theta)$ are actually quasi two-dimensional, and the θ coordinate is a parameter. These equations are complementary. If all integrands of u_i^h variation [first two lines of (9)] are zero, then s_{ij}^h satisfies the same traction boundary conditions and truncated equilibrium equations as

$\sum_{p=1}^{N-1} K_p(\theta) s_{ij}^{a,p}$. If these equations are satisfied under displacement boundary condition

$$u_i^h = \sum_{p=1}^{N-1} K_p(\theta) u_i^{a,p}, x_i \in \partial \Gamma_V,$$

then by simple manipulations of the energy equations obtained by varying $K_p(\theta)$, one can prove that they will be satisfied identically for arbitrary $K_p(\theta)$. Due to the linear type of traction and displacement boundary conditions and the quasi two-dimensional character of equations for u_i^h , one can represent the solution as

$$u_i^h = \sum_{p=1}^{N-1} K_p(\theta) u_i^{h,p}.$$

Without restricting generality, the approximation of $u_i^{h,p}$ is also based on basis functions (6)

$$u_i^{h,p} = u_{im}^{h,p} \chi_i^m(x_i),$$

where some of the coefficients $u_{im}^{h,p}$ are fixed so that the boundary conditions

$$u_i^{h,p} = u_i^{a,p}, x_i \in \partial\Gamma_V$$

are satisfied for $p=1, \dots, N-1$. Taking into account the displacement approximation expressions,

we derive the following system of equations for determination of the coefficients u_{im} and $u_{im}^{h,p}$

$$\begin{aligned} \iiint_V \sigma_{ij} \chi_{i,j}^m dv - \iint_{\Gamma_t} T_i \chi_i^m ds &= 0, \\ m &= 1, 2, \dots \\ \iiint_V s_{ij}^{h,p} \chi_{i,j}^m dv - \iiint_V s_{ij}^{a,p} \chi_{i,j}^m dv &= 0 \\ m &= 1, 2, \dots \text{ and } p = 1, \dots, N-1. \end{aligned} \quad (10)$$

where

$$\sigma_{ij} = \frac{1}{2} C_{ijkl} (u_{km}^i \chi_{k,l}^m + u_{lm}^i \chi_{l,k}^m)$$

and

$$s_{ij}^{h,p} = \frac{1}{2} C_{ijkl} (u_{km}^{h,p} \chi_{k,l}^m + u_{lm}^{h,p} \chi_{l,k}^m)$$

Note that the fixed coefficients u_{im}^0 also enter the equations and form an effective load vector additional to the traction loading.

The first system of equations fully defines the total displacement (2) independently of u_i^h and $K_p(\theta)$. In the case of the polynomial approximation (6), the obtained displacements will not provide zero values of all three integrands in the last two lines of the variational equation (9) in

the vicinity of the intersections $\partial V_i \cap z = z^{(p)}$. Practically, we will observe traction discontinuity at the interfaces near the hole edge and the traction boundary condition error at the hole edge for the stress field σ_{ij} calculated using full displacement. It also follows that the equilibrium equations will not be satisfied. This is a result of approximating a directionally nonunique singular stress field (5) by polynomials. The directional nonuniqueness means that for $\eta \rightarrow 0$, the stresses $s_{ij}^{a,p}$ may tend to be plus or minus infinity depending upon ψ . The polynomial approximation provides a unique and finite stress value at every point of a given ply. The values of the stress intensity factors are obtained to satisfy the condition of directional uniqueness of the polynomial part of $\bar{\sigma}_{ij}$ at the singular point. Consider the interface $z = z^{(p)}$ and the p -th ply. Let $P_i^{(p)}$ be the exact value of the interlaminar traction on the interface $z = z^{(p)}$. Then at the hole edge six conditions have to be simultaneously satisfied

$$T_i = \bar{\sigma}_{ij} n_j^h, P_i^{(p)} = \bar{\sigma}_{ij} n_j^p,$$

wherein polar coordinates $n_1^h = n_3^p = 1$, and all other components of the two normal vectors, are equal to zero. Taking into account Equation (7) one can write

$$\begin{aligned} & \lim_{\eta \rightarrow 0} (T_3 - K_p(\theta) s_{rz}^{a,p}(\eta, \frac{\pi}{2}, \theta)) \\ &= \lim_{\eta \rightarrow 0} (P_1 - K_p(\theta) s_{rz}^{a,p}(\eta, 0, \theta)) \\ &= \sigma_{rz}^B(\frac{D}{2}, z^{(p)}, \theta) \end{aligned} \quad (11)$$

where the polynomial part of the stress tensor is given by equation:

$$\sigma_{ij}^B = \sigma_{ij} - s_{ij}^h$$

These equations are necessary conditions of directional uniqueness of the polynomial part of the stress tensor. In the case of an open hole, $T_i=0$, the first limit in equation (11) yields that

$$\sigma_{rz}^B\left(\frac{D}{2}, z^{(p)}, \theta\right) = 0, p = 1, \dots, N-1.$$

This condition provides the following equations for determining $K_p(\theta)$.

$$\begin{aligned} \sigma_{rz}\left(\frac{D}{2}, z^{(p)}, \theta\right) &= \sum_{q=1}^{N-1} K_q(\theta) s_{ij}^{h,q}\left(\frac{D}{2}, z^{(p)}, \theta\right), \\ p &= 1, \dots, N-1 \end{aligned} \quad (12)$$

where

$$s_{ij}^h = \sum_{p=1}^{N-1} K_p(\theta) s_{ij}^{h,p}.$$

The second limit in (11) cannot be enforced. However, if the exact solution can be represented according to (7), i.e., the nonpolynomial terms are correct, then both equations (11) should be satisfied for the same $K_p(\theta)$. It is worth noting that if instead of a corner one has a crack, i.e., $n_i^h = -n_i^p$, then we shall have three pairs of directional uniqueness conditions, one per each stress component in the plane normal to the crack. It will require three stress intensity factors: Mode I, II and III.

1.5 Spline Approximation of Displacement Components

A detailed description of the spline approximation procedure and the properties of spline functions are given by Iarve [9]. The x,y plane was mapped into a rectangular region ρ, ϕ , where $0 \leq \rho \leq 1$ and $0 \leq \phi \leq 2\pi$. The transformation was defined as follows:

$$\begin{aligned}
x &= \frac{D}{2} F_1(\rho) \cos \phi + L \cdot F_2(\rho) \alpha(\phi) + x_c \\
y &= \frac{D}{2} F_1(\rho) \sin \phi + A \cdot F_2(\rho) \beta(\phi) + y_c
\end{aligned} \tag{13}$$

Functions F_1 and F_2 were defined as

$$F_1(\rho) = \begin{cases} 1 + \kappa \cdot \rho, & \rho \leq \rho_h \\ \frac{(1 + \kappa \cdot \rho_h)(1 - \rho)}{1 - \rho_h}, & \rho_h \leq \rho \leq 1 \end{cases} \quad F_2(\rho) = \begin{cases} 0, & \rho \leq \rho_h \\ \frac{\rho - \rho_h}{1 - \rho_h}, & \rho_h \leq \rho \leq 1 \end{cases}$$

This transformation was defined so that the coordinate line $\rho=0$ describes the contour of the hole, and the coordinate line $\rho=1$ describes the rectangular contour of the plate. Inside the near-hole region $D/2 \leq r \leq (1+\kappa)D/2$, which corresponds to $0 \leq \rho \leq \rho_h$, a simple relationship between the polar coordinates and the curvilinear coordinates ρ , ϕ exists:

$$r - \frac{D}{2} = \frac{D\kappa}{2} \rho \quad \text{and} \quad \theta = \phi. \tag{14}$$

The width of this region is typically two hole radii, i.e., $\kappa\rho_h = 2$. Beyond this region a transition between the circular contour of the opening and the rectangular contour of the plate is performed. Functions $\alpha(\phi)$ and $\beta(\phi)$ describing the rectangular contour of the plate boundary were given by Iarve [9]. These functions are introduced so that parametric equations $x=\alpha(\phi)+x_c$, $y=\beta(\phi)+y_c$ describe the rectangular contour of the plate, and $0 \leq \phi < \phi^{(1)}$ corresponds to $0 < x \leq L, y=A$; $\phi^{(1)} \leq \phi < \phi^{(2)}$ corresponds to $x=0, 0 < y \leq A$; $\phi^{(2)} \leq \phi < \phi^{(3)}$ corresponds to $0 \leq x < L, y=0$ and $\phi^{(3)} \leq \phi < 2\pi$ corresponds to $x=L, 0 \leq y < A$.

The spline approximation of displacement and interlaminar stress components in curvilinear coordinates was utilized. Subdivisions were introduced through the thickness of each ply

$$z^{(s-1)} = z_0 < z_1 < z_2 < \dots < z_{n_s} = z^{(s)}$$

where $s=1, \dots, N$ -total number of plies. The s -th ply occupies a region $z^{(s)} \leq z \leq z^{(s-1)}$, and n_s is the number of sublayers in the s -th ply. Nodal points are also introduced in the ρ and ϕ directions as follows: $0 = \rho_0 < \rho_1 < \dots < \rho_m = 1$, $0 = \phi_0 < \phi_1 < \dots < \phi_k = 2\pi$. The subdivision of the ρ coordinate is essentially nonuniform. The interval size increases in geometric progression beginning at the hole edge. The region $0 \leq \rho \leq \rho_h$ in which the curvilinear transformation is quasi polar is subdivided into m_0 intervals, so that $\rho_h = \rho_{m_0}$. Sets of basic B-type cubic spline functions $\{R_i(\rho)\}_{i=1}^{m+3}$, $\{\Phi_j(\phi)\}_{j=1}^{k+3}$, $\{Z_l(z)\}_{l=1}^{N_z}$, $N_z = \sum_{s=1}^N n_s + 2N + 1$, along each coordinate are built according to recurrent procedures given by Iarve [9]. Splines along the ϕ coordinate have periodical properties at the ends of the interval. The three-dimensional approximation of displacement components was written using the tensor product of three one-dimensional sets of splines. The vector of the three-dimensional spline approximation functions was defined as:

$$\begin{aligned} \{\bar{\chi}\}_q &= R_i(\rho) \Phi_j(\phi) Z_l(z), \\ q &= l + (j-1)N_z + (i-1)N_z k, \\ l &= 1, \dots, N_z, j = 1, \dots, k, i = 1, \dots, m+3. \end{aligned}$$

Since the orthotropic material properties become location dependent in the curvilinear coordinate system, the displacement components were considered relative to x , y and z as functions of ρ , ϕ and z . The following approximation was used

$$u_i = \mathbf{C}_i \bar{\chi} \mathbf{U}_i^* + \delta_{1i} \bar{\chi} \mathbf{E}^* \cdot u_0 \quad (15)$$

Bold type will be used to distinguish vectors and matrices; superscript star means transpose operation. Vectors \mathbf{U}_i contain unknown displacement spline approximation coefficients. Non-square boundary matrices $\mathbf{C}_1, \mathbf{C}_2, \mathbf{C}_3$ and constant vector \mathbf{E} are defined so that the approximation (15) provides a kinematically admissible, i.e., satisfying boundary conditions (1), displacement field for any coefficients \mathbf{U}_i . The components of vector \mathbf{E} are equal to 1 or -1 if the same component of $\bar{\chi}$ is nonzero at $\rho=1, \phi^{(1)} \leq \phi < \phi^{(2)}$ ($x=0$) and $\rho=1, \phi^{(3)} \leq \phi < 2\pi$ ($x=L$), respectively. All other components of the vector \mathbf{E} are equal to zero. The boundary matrices are obtained by deleting a number of rows from the unit matrix. The deleted rows have nonzero scalar product with \mathbf{E} .

The region Γ of the hybrid approximation superposition is inside the region in which the transformation (13) coincides with (14). The boundary $\partial\Gamma_v$ is concentric with the hole edge and is defined by equation $r = \frac{D}{2} (1 + \kappa \rho_{m_h})$, where $m_h \leq m_0$. For the purposes of efficient solution of the systems of equations for determining $u_i^{h,p}$, a reduced set of splines in the ρ direction

$\{R_i^h(\rho)\}_{i=1}^{m_h+3}$ defined only over the first m_h intervals is utilized. It is built exactly the same way as the one over the entire interval. It can be shown that the reduced set is a subset of the approximation (15). The approximation of the hybrid portion of the displacements can be written as

$$u_i^{h,p} = \mathbf{C}_i^{h,p} \bar{\chi}^h \mathbf{U}_i^{h,p*} + \bar{\chi}^h \mathbf{U}_i^{a,p*} \quad (16)$$

where $\mathbf{U}_i^{h,p}$ are unknown coefficients and

$$\begin{aligned}\left\{\bar{\chi}\right\}_q &= R_i^h(\rho)\Phi_j(\phi)Z_l(z), \\ q &= l + (j-1)N_z + (i-1)N_z k, \\ l &= 1, \dots, N_z, j = 1, \dots, k, i = 1, \dots, m_h + 3.\end{aligned}$$

The coefficients of $\mathbf{U}_i^{a,p}$ are nonzero only if the respective component of $\bar{\chi}^h$ is nonzero at

$\rho = \rho_{m_h}$. The vectors $\mathbf{U}_i^{a,p}$ are defined so that

$$u_i^{a,p} = \bar{\chi}^h \mathbf{U}_i^{a,p*}, \rho = \rho_{m_h}$$

It is possible to do with high accuracy if $r = \frac{D}{2}(1 + \kappa\rho_{m_h})$ is sufficiently far from the hole edge. The

matrices $\mathbf{C}_1^{h,p}$ are derived from unit matrices similar to those in (15) by treating vectors $\mathbf{U}_i^{a,p}$

analogously to vectors \mathbf{E} . The truncated in-plane derivatives are calculated as:

$$\frac{\partial}{\partial \bar{x}} = \frac{2}{D\kappa} \cos \phi \frac{\partial}{\partial \rho}, \frac{\partial}{\partial \bar{y}} = \frac{2}{D\kappa} \sin \phi \frac{\partial}{\partial \rho},$$

The final outline of the solution procedure is as follows. Approximations (15) and (16) are substituted into Equation (10). The vectors of unknown coefficients of total displacement approximation \mathbf{U}_i and the hybrid components $\mathbf{U}_i^{a,p}$ are determined. Then the stresses at the hole edge on the ply interfaces are calculated and finally the stress intensity factors $K_p(\theta)$ obtained by using Equation (12). The solution is complete and Equation (7) can be applied to provide accurate stress values including singularities.

1.6 Numerical Results

A square $[45/-45]_s$ plate similar to that in Wang and Lu [8] is considered. The geometric properties are $L=A=20$ in., $x_c=y_c=L/2$, $D=2$ in., ply thickness $h=0.1$ in. $E_1=20$ Msi, $E_2=E_3=2.1$

Msi, $G_{12} = G_{13} = G_{23} = 0.85$ Msi and $\nu_{12} = \nu_{13} = \nu_{23} = 0.21$. The ply properties are used for comparison purposes only and are not associated with a realistic material system. The displacement boundary conditions were applied so that $u_0/L = 0.001$. The average applied stress was calculated as

$$\sigma_0 = \frac{1}{AH} \iint_{z,y} \sigma_{xx}(L, y, z) dx dz$$

Several subdivisions were used for the convergence study. The θ coordinate in all cases was uniformly divided into 48 intervals. The subdivisions of the ρ coordinate were:

- (i) a total of $m=16$ intervals, with $m_0=12$ intervals in the quasi cylindrical transformation region, which was a hole radii wide ($\kappa\rho_h = 1$); the consecutive interval length ratio was $q=1.2$.
- (ii) $m=24$, $m_0=20$, $\kappa\rho_h = 1$, $q=1.4$.

The subdivisions in the z -direction were also nonuniform and symmetric against the interface:

- (i) $n_s=1$, one sublayer per ply.
- (ii) $n_s=2$, the sublayer closest to midsurface was 1.3 times thinner than the outer one.
- (iii) $n_s=4$, sublayer thickness ratio 1.3.

First, the influence of the width of the region Γ on the value of the stress intensity factor is investigated. Subdivision into two sublayers per ply and 16 intervals were used. The width of the region m_h was changed from 1 to 12 intervals. The stress intensity factor $K(\theta)$ in units $\text{psi} \times \text{in}^{(1-\lambda(\theta))}$ divided by the applied load σ_0 is shown in Figure 2a. Starting with $m_h=4$ the $K(\theta)$ values are practically unchanged. It should be noted that the minimum value, even for $m_h=1$, is different from the value obtained for $m_h \geq 4$, only 12 percent. In all of the following results, $m_h=10$. Figure 2b illustrates the influence of the density of subdivision on the $K(\theta)$ values. A small

difference between the results obtained with the limiting meshes can be seen for θ angles around 45° and 135° where the stress intensity factor is small. A qualitative agreement between the present results and Wang and Lu [8], also shown in Figure 2b, is observed.

Stress results obtained by using the hybrid approximation will be illustrated below. The r_z and z_z stress components in the cross section $\theta=90^\circ$ will be considered at the interlaminar surface. The shear stress σ_{rz} distribution calculated from the total displacements is shown in Figure 3a for two different subdivisions.

For distances from the hole edge smaller than $0.4H$ and $0.9H$ for the finer and coarser subdivisions, respectively, the shear stress is discontinuous at the interface. Mesh refinement will further shrink the distance at which the discontinuity is visible; however, the stress values at the hole edge on the two-ply surfaces will diverge even more. This behavior is readily understood by examining the asymptotic stress functions (5). The functions $s_{ij}^a(1, \psi, 90^\circ)$ are

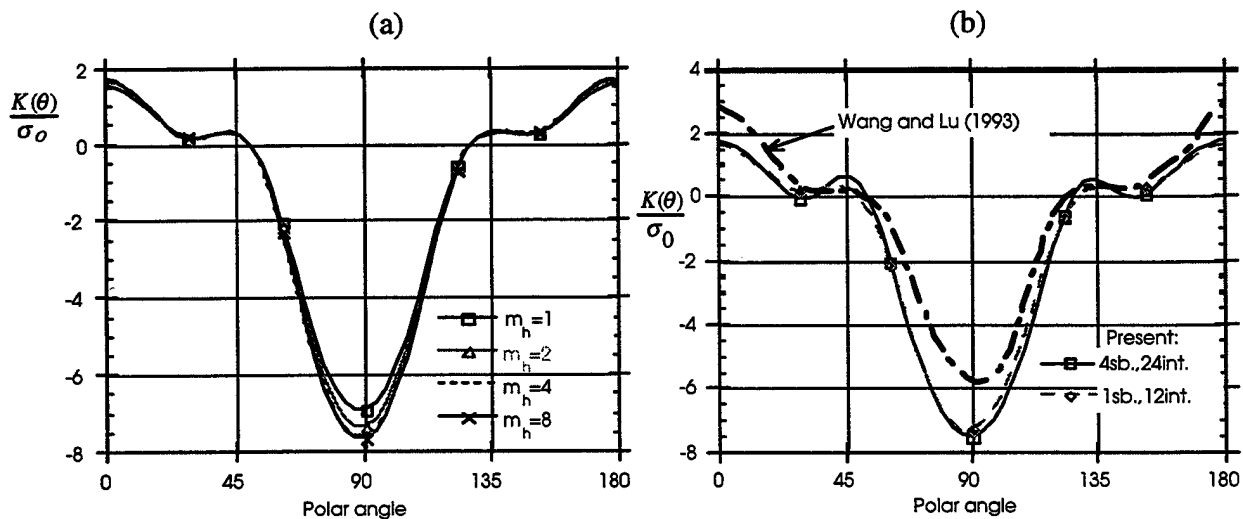


Figure 2. Stress Intensity Factor for Different Superposition Region Sizes (a) and Different Subdivisions (b).

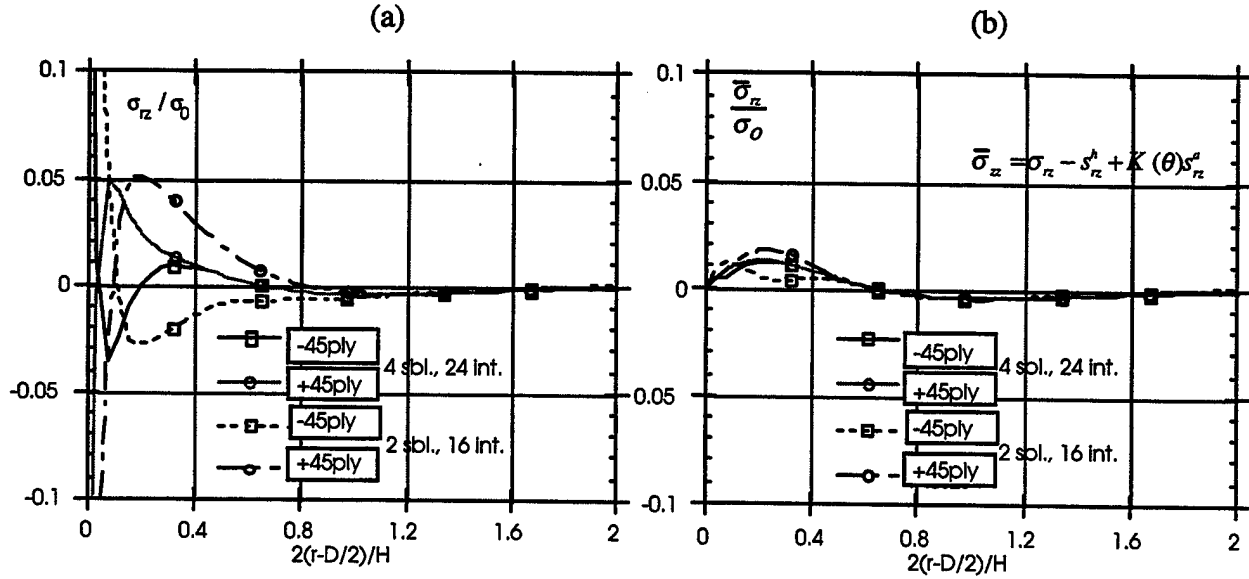


Figure 3. Shear Stress Calculated Using Total Displacement (a) and the Hybrid Expressions (b).

shown in Figure 4. The angular distribution of the shear component $s_{rz}^a(1, \psi, 90^\circ)$ satisfies the zero boundary conditions at the hole surfaces $\psi = \pm\pi/2$ and the continuity condition at the interface $\psi = 0$. In addition the stress amplitude along the interface is zero which means the

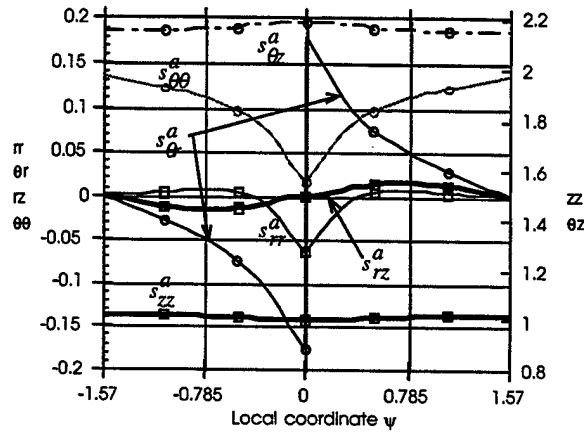


Figure 4. Angular Distribution of the Asymptotic Stress Functions.

stress is not infinitely growing if the singular point is approached in this direction. Within the plies, the same stress component is unbounded at the same point, and tends to be minus infinity in the lower ply and plus infinity in the upper ply. The directional nonuniqueness of the solution

is reflected by diverging the interlaminar shear stress value given by the polynomial approximation (Figure 3a). The stresses calculated by using Equation (7) are shown in Figure 3b and clearly indicate convergence with mesh refinement. Note that the stress displayed on this figure is at the same time the pure polynomial part of the hybrid stress, since $s_{rz}^a(1, \psi, 90^\circ) = 0$. Thus, by approaching the singular point along the hole edge, we will again recover the zero value. Inside the plies infinite stresses will result due to the presence of a singular term in the hybrid approximation.

Finally, the transverse normal stress component will be considered. As seen in Figure 4, it exhibits a practically constant directional amplitude in the $\theta = 90^\circ$ cross section. The stress values σ_{zz} defined through the total displacement field by using the same two meshes as before are shown in Figure 5a. For both meshes no discontinuity between the stress values in the two plies at the interface can be seen. However, the stress values obtained using the coarse and the fine mesh are different in the hole edge vicinity. Figure 5b displays the quantity

$$K(\theta)s_{zz}^a - s_{zz}^h$$

which is superimposed to the displacement-based stress value in Equation (7). For the fine mesh it has a nonzero value only in the very vicinity of the singularity and extends up to $0.9H$ away from the hole edge for the coarse mesh. The hybrid stress values $\bar{\sigma}_{zz}$ for the two meshes are shown in Figure 5c and display remarkable agreement.

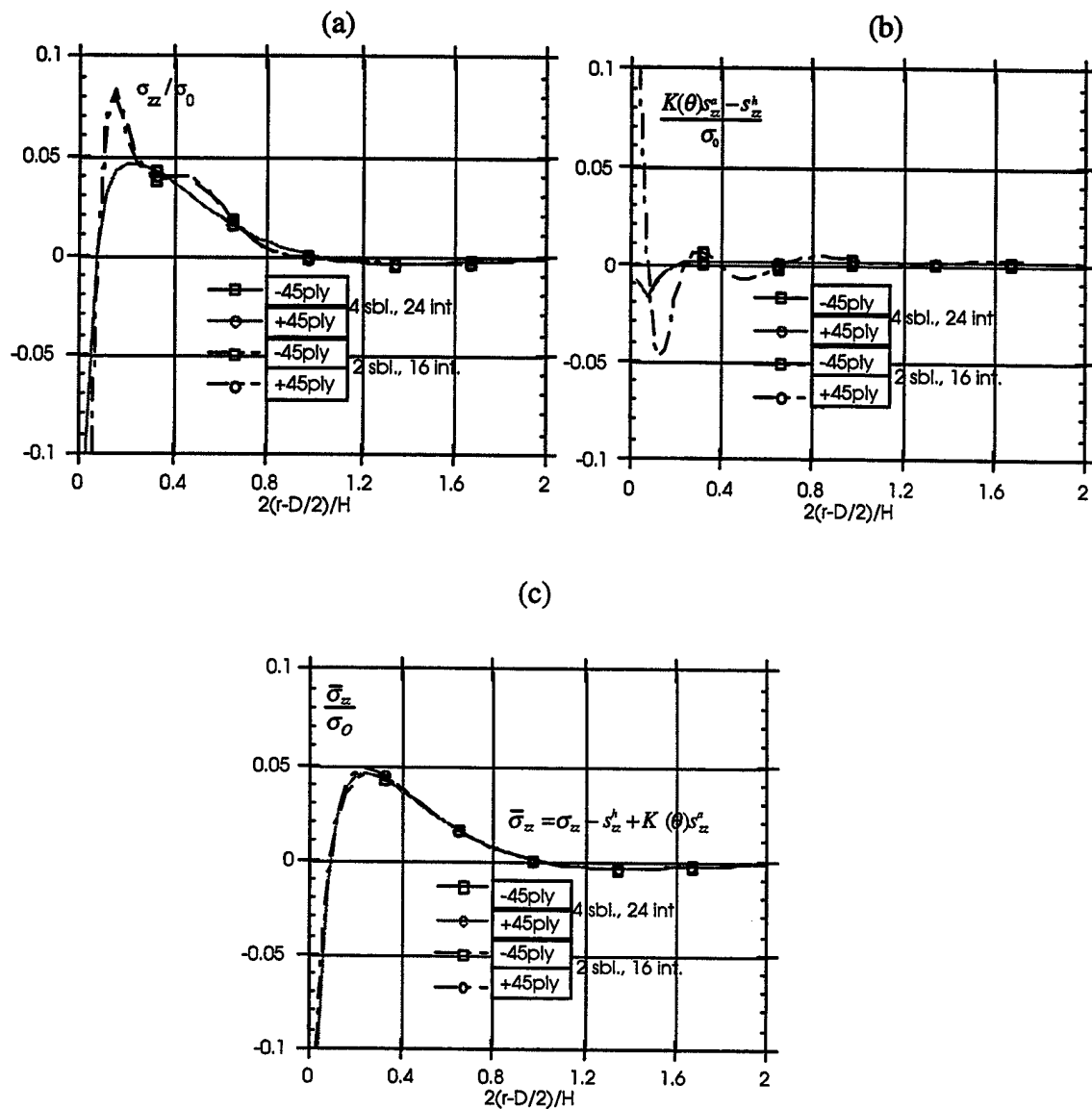


Figure 5. Transverse Normal Stress σ_z -(a), $K(\theta)s_z^a - s_z^h$ -(b), and the Hybrid Approximation Stress $\bar{\sigma}_z$ -(c).

2. DAMAGE INITIATION AND PROGRESSION FOR BASIC LAMINATES WITH A HOLE

The occurrence of holes in load-bearing composite structures is pervasive in the aerospace industry as a result of the use of mechanical fasteners in assembly and the use of cutouts to accommodate wiring and hydraulic lines. The design of laminates with holes or with fasteners in composite structures is largely based on experimental test data (Shyprekevich [14]). The most widely utilized analysis methods are those based on the two-dimensional elasticity solution provided by Lekhnitskii [15] for an infinite orthotropic plate with an open hole. These methods, including the model of Garbo and Ogonowski [16], are summarized by Snyder *et al.* [17]. In an effort to model the fastener, Lekhnitskii assumes a cosine distribution of radial tractions and a contact zone size. Although the aforementioned analyses are useful design tools, a more rigorous stress analysis method and failure criterion are needed to predict the strength of laminates with holes and with fasteners.

Recently, Iarve [9,18] developed a three-dimensional stress analysis method for a composite laminate with an open hole or an elastic inclusion. This method is based on the spline variational theory and was verified through comparisons of in-plane and interlaminar stresses with results obtained from an asymptotic solution. Results presented herein were determined using Spline Variational Elastic Laminate Technology (SVELT), a dedicated computer package which implements the analysis described by Iarve [9,18].

A number of experimental studies have documented the progression of damage for composite laminates with open holes. Shalev and Reifsnider [19] presented observations on the onset of delamination, while transverse cracking was the focus of works by Joshi and Huang [20] on quasi-isotropic laminates and Reddy *et al.* [21] on cross-ply laminates. Lessard and Chang

[22] discuss the development of damage in laminates containing open holes for tension. In these works, observations were not made in a building block fashion for both unidirectional and basic laminates.

In this two-part work, quasi-static loading experiments were conducted on basic laminates to document the initiation and growth of damage and to record changes in the strain field. The objective of this work was the development of an experimental database from which three-dimensional stress analysis methods with discrete damage and associated failure criterion are later investigated and verified. In part I of this work, three IM7/5250-4 laminates, $[0_8]_T$, $[90_8]_T$, and $[\pm 45]_{2S}$, were incrementally loaded to failure. For each loading increment, axial strain was recorded in close proximity to the hole, and the specimen was x-rayed. Acoustic emission data were collected during loading and compared to strain measurements and radiographic images to identify significant damage events. Additional analysis was conducted by comparing experimental strain data to results obtained from elasticity theory and from spline variational theory. Part II of this work is in progress and considers more complex laminates.

2.1 Experiment

A series of tension tests were conducted to document the initiation and propagation of damage in basic composite laminates with a centrally located circular hole. Of particular interest is the response of IM7/5250-4. Testing was conducted in two phases: monotonic loading of unnotched tensile coupons to failure and incremental loading of open-hole specimens to failure. The purpose of the first phase is to obtain mechanical properties including stiffness and strength in the transverse and longitudinal directions. The purpose of the second phase is to document the progression of damage and the corresponding strain response. Three laminate orientations were

considered: $[0_8]_T$, $[90_8]_T$, and $[\pm 45]_{2S}$. Each laminate was cured according to the manufacturer's recommended cure cycle and was postcured at 227°C (440°F) for a duration of five hours and 40 minutes. The average fiber volume was reported as 62 percent based on procedures established in ASTM 3171-76, and the void content was determined to be less than one percent.

For the monotonic loading phase, the nominal tensile coupon dimensions were 2.54 cm wide, 30.48 cm long with a tab length of 2.54 cm for the $[90_8]_T$ and the $[\pm 45]_{2S}$ laminate. A variation of this specimen was used for the $[0_8]_T$ laminate, where the coupon width was 1.27 cm. The average ply thickness was determined to be 0.134 mm (0.00527 in.). A total of six specimens were tested for $[0_8]_T$ and $[90_8]_T$ laminates, while three replicate tests were conducted for the $[\pm 45]_{2S}$ laminate. Measurements of axial and transverse strains were recorded for each specimen using strain gages during loading. Results of the monotonic tensile testing are summarized in Table 1.

TABLE 1
Summary of Mechanical Properties for Basic Laminates

Laminate	Modulus, GPa	Strength, MPa	Strain to failure, %
$[0_8]_T$	151	2640	1.5
$[90_8]_T$	10.7	68.9	0.68
$[\pm 45]_{2S}$	21.4	208	>3.0

For the incremental loading phase, an open-hole tension specimen is utilized with the following specimen dimensions: $L=30.48$ cm, $W=7.62$ cm, tab length =2.54 cm, and hole diameter $D=1.27$ cm. A longer tab length, 3.81 cm, is selected for the $[0_8]_T$ laminate to avoid tab debonding. Prior to initial loading, no transverse cracks were observed upon radiographic inspection of each specimen. Each specimen was monotonically loaded to a value P_1 and then

unloaded. Axial strains were recorded during the test using up to six strain gages, while acoustic emission measurements were monitored to identify potential damage events. Typically, two strain gages were employed in the far-field region, and four strain gages were arranged to record the strain intensity approaching the hole edge perpendicular to the loading direction. The load P_1 was either a predetermined value based on assumed ply behavior, usually well below the anticipated transverse cracking stress, or a value corresponding to a significant acoustic event after which the specimen was unloaded. Following loading of the specimen to a value, P_1 , the specimen was x-rayed in the unloaded condition to document evidence of damage. This process was repeated for increasing loads P_2 , P_3 , etc. until failure.

A description of the drilling procedure is provided to emphasize the importance of minimizing drill-induced damage. A carbide-tipped steel drill bit with an operating speed of 800 rpm was selected for specimen fabrication procedures. This type of bit is specially designed for cutting holes for layered media such as circuit boards. Surface damage was minimized by using glass/epoxy laminates on the top and bottom surface of the specimen prior to drilling. This drilling process produced holes that were absent of transverse cracks for nine out of ten holes. It is important to note that drilling-induced damage cannot be totally eliminated. Utilizing similar procedures, Schaff, *et al.* [23] showed that damage exists in the form of chipping and is visible in the surface ply around the hole periphery extending away from the edge a distance of one ply thickness. These regions were rarely more than a few fiber diameters in depth through-the-thickness of the ply and typically occurred where fibers approach the edge at a large angle.

2.2 Results and Discussion

2.2.1 Analysis

SVELT is based on the spline approximation of displacements u , v , and w in terms of unknown spline coefficients and sets of basic spline functions. Displacements, interlaminar tractions, and prescribed tractions are used to construct a system of equations by applying the minimum potential energy principle. After displacement boundary conditions are enforced, the remaining set of equations can then be solved for the unknown spline coefficients. Strains are determined from displacement relations and are continuous within a ply. The spline geometry utilized to obtain the present results is given by $n'=3$, $k'=72$, $m'=22$, $m'_0=16$, and $q=1.4$ according to the convention described by Schaff, *et al.* [23].

Two-dimensional results were obtained using the elasticity solution for an orthotropic plate with a circular hole [15]. All stress analysis results were obtained using the following properties: $E_{11}=151$ GPa, $E_{22}=E_{33}=10.7$ GPa, $G_{12}=G_{23}=5.9$ GPa, $G_{13}=3.26$ GPa, $\nu_{12}=\nu_{23}=0.309$, $\nu_{13}=0.449$, $\alpha_{11}=0.61 \times 10^{-6}/^{\circ}\text{C}$ and $\alpha_{22}=25.2 \times 10^{-6}/^{\circ}\text{C}$.

2.2.2 $[90_8]_T$ Laminate

The $[90_8]_T$ laminate was subjected to two loading increments: 23.7 MPa (3.44 ksi) and 32.7 MPa (4.74 ksi). The last loading corresponds to the failure load. It is apparent from acoustic emission sensors and strain measurements that initiation of a transverse crack and specimen failure occurred simultaneously. Inspection of the post-failed specimens indicates net tension failure perpendicular to the loading axis in the hole ligament. The location of the failure is described by transverse cracks at approximately 87° and 270° clockwise from the top of the specimen along the loading direction, hereafter referred to as the reference direction. Figure 6 shows the stress-strain curves obtained from four strain gages (e_1 , e_2 , e_3 , and e_4) in close

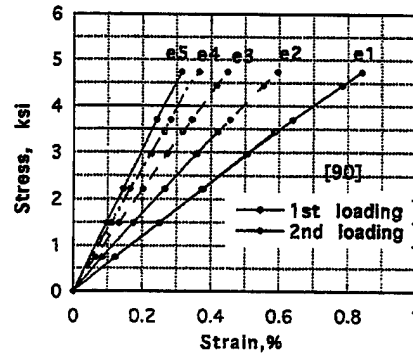


Figure 6. Stress-Strain Curves from Gages e1-e5 for $[90]_T$ Laminate.

proximity to the hole and for the far-field strain gage (e5). Gage e1 is inside the hole, and e2, e3, and e4 are centered at distances 0.127 cm (0.05 in), 0.381 cm (0.15 in), and 0.889 cm (0.35 in) away from the hole edge perpendicular to the loading direction. Strains e2 to e5 are linear up to failure, whereas strain on the hole edge, e1, is initially linear and exhibits slightly nonlinear behavior at approximately 0.6 percent strain. This value of strain is close to the failure strain of the unnotched tensile coupons, 0.68 percent. The strain recorded from gage e1 is 0.84 percent at failure which is 25 percent greater than the strain to failure reported in Table 1.

In Figure 7 the axial strain from SVELT and from experiment (e2, e3, and e4) are plotted perpendicular to the direction of loading and along a radial path beginning at the hole edge and extending to $12.5T_{lam}$ where T_{lam} is 0.114 cm (0.045 in). Comparisons are made for applied stress values of 10.2 MPa (1.48 ksi), 15.3 MPa (2.22 ksi), 20.4 MPa (2.96 ksi), and 23.8 MPa (3.45 ksi). In general, good agreement between SVELT and experiment is observed. Strain concentration factors at the hole edge can be determined by the strain ratio $e1/e5$ and compared to those determined by SVELT and Lehnitskii. The range of values of $e1/e5$ at low loadings is calculated as 2.54-2.65, which agrees well with those obtained from SVELT and elasticity, i.e., 2.66 and 2.54, respectively.

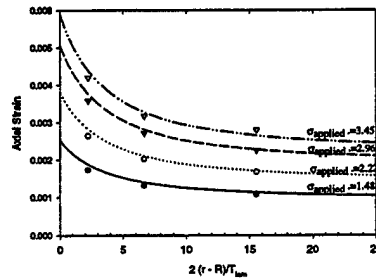


Figure 7. Comparison of Strain Measurements with Axial Strain from SVELT.

2.2.3 $[0_8]_T$ Laminate

The $[0_8]_T$ specimen was subjected to nine load steps where each step is defined by the following peak values of applied stress: 183.9 MPa (26.67 ksi), 229.8 MPa (33.33 ksi), 270.7 MPa (39.26 ksi), 332.0 MPa (48.15 ksi), 510.7 MPa (74.07 ksi), 766.1 MPa (111.1 ksi), 1277 MPa (185.2 ksi), 1787 MPa (259.2 ksi), and 2119 MPa (307.3 ksi). Laminate failure occurred in net tension during the ninth load step at an applied stress of 2119 MPa (307.3 ksi). A description of the onset of damage and the subsequent growth of damage is discussed with the aid of radiographic images and stress strain curves for selected loadings. In Figures 8a through 8e, radiographic images following load steps 1, 2, 3, 4 and 8 are presented as a direct indication of the damage state. The $[0_8]_T$ laminate used the same arrangement of strain gages as the $[90_8]_T$ specimen, except two strain measurements were recorded in the far-field region. Inspection of Figure 8 shows two far- field strain gages at the bottom of the specimen, where gage e5 is centered and gage e6 is closer to the edge. In Figure 8 a strain gage wiring post is positioned close to the hole and 135° clockwise from the reference direction. The experimentally-measured stress-strain results are shown for load steps 1, 2, 3, 4, 5, and 9 in Figures 9a through 9f,

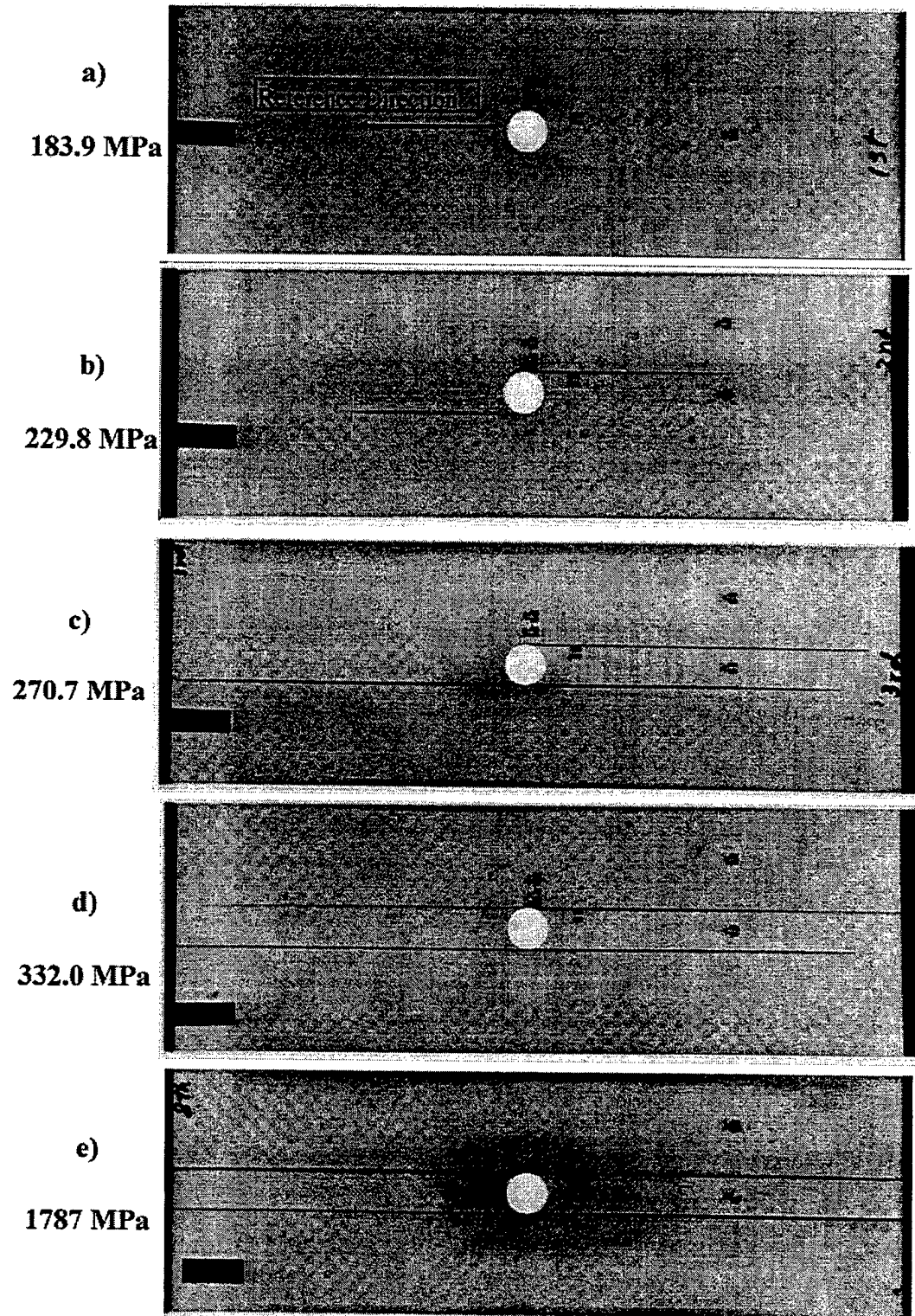


Figure 8. Radiographic Images of [0_g]_T Specimen for Load Steps 1-4 and 8.

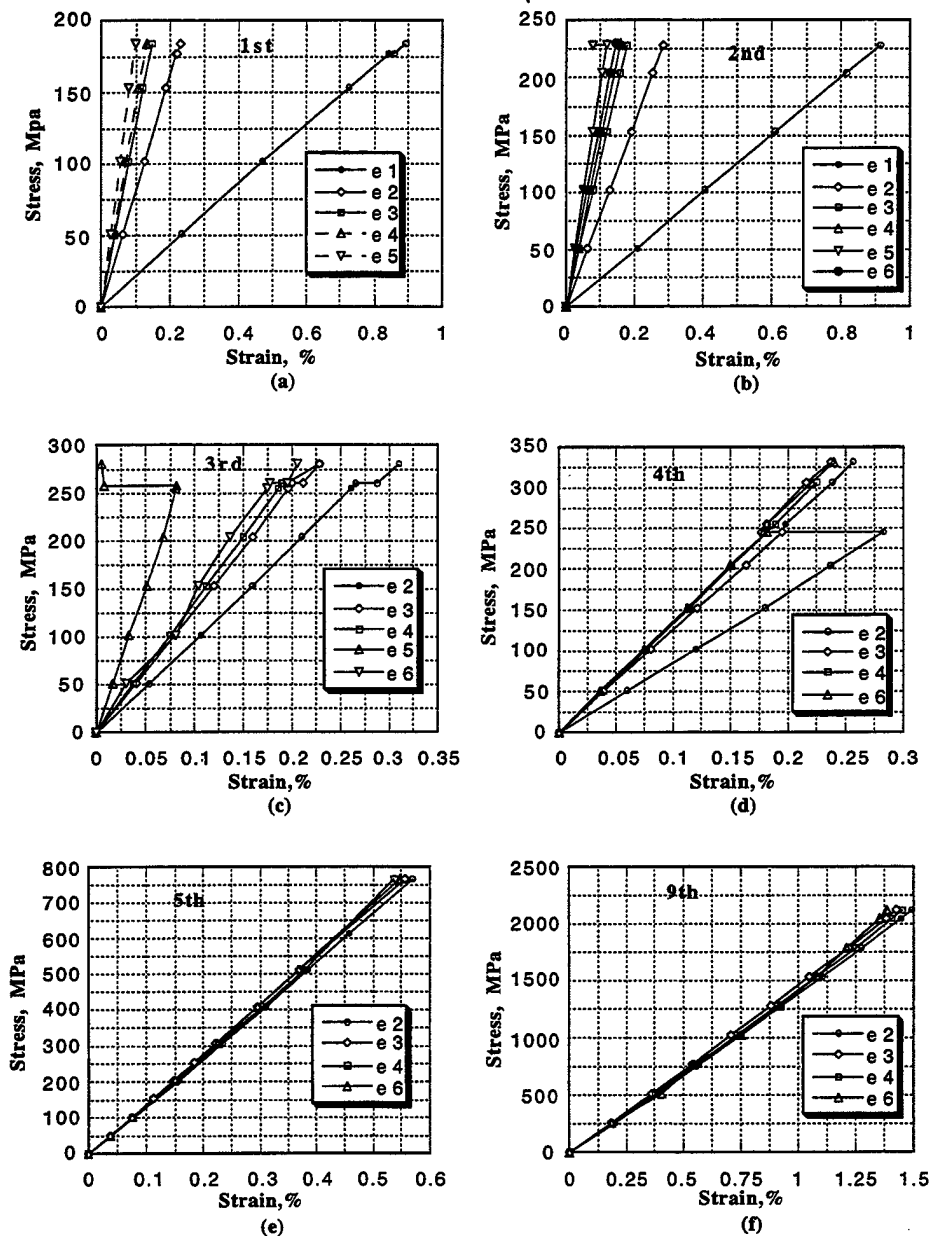


Figure 9. Stress-Strain Curves for Gages e1-e6 for $[0]_T$ Laminate at Load Steps: (a) 183.9 MPa (26.67 ksi), (b) 229.8 MPa (33.33 ksi), (c) 270.7 MPa (39.26 ksi), (d) 332.0 MPa (48.15 ksi), (e) 510.7 MPa (74.07 ksi), and (f) 2119 MPa (307.3 ksi).

respectively. Results are provided for all gages in close proximity to the hole, e1 through e4, and gages in the far-field region, e5 and e6. Gage e1 was recorded for only the first two load steps due to inadequate strain gage capacity.

The first transverse crack emitted from the hole edge approximately 277° clockwise from the reference direction. Inspection of Figure 8a reveals that a transverse crack 6 mm in length appeared after the first loading step, 183.9 MPa (26.67 ksi). It is speculated that the crack initiated at a stress of 174 MPa (25.24 ksi) based on the first acoustic emission peak. In general the effect of the transverse crack was not evident in the measured strain data, because the crack and the strain gages are located on opposite sides of the hole. However, strain gage e1 showed a slight increase at 176 MPa (25.53 ksi) which coincided with the first acoustic peak, 174 MPa (25.24 ksi).

The second transverse crack occurred at the end of load step 2 and is shown in Figure 8b. For this load step the specimen was unloaded at the first signal of activity from the acoustic emission sensor. Strains e1 and e5 show erratic behavior in Figure 9b at the end of the second loading. Inspection of the x-ray radiograph for load step 3 exhibits the development of the third crack at 263° clockwise from the reference direction and extends within 1 cm of the end tab. Figure 8c also shows the onset of this new crack and the growth of two previous transverse cracks to the tab region. During the third load step, the strain e1 exceeded the gage capacity at an applied stress of 257.9 MPa (37.40 ksi). Almost simultaneously, a drop of strain e5 to near zero indicates stress relaxation in the center strip portion bounded by transverse cracks, i.e., the load carried by the mid-strip was transferred to the edge ligaments. Furthermore, the load transfer is also detected by the increase of strains e2, e3, e4, and e6 as shown in Figure 9c. The final

transverse crack developed near strain gage e2 at approximately 83° clockwise from the reference direction during load step 4 at a stress of 245.1 MPa (35.55 ksi).

Figure 10 displays the experimental stress strain curves for gage e2 for load steps 1-9. Note that the e2 strain behavior is nearly identical after load step 4. The average moduli obtained from e2 for load steps 5-7 were determined to be within one percent of the experimental value from unnotched coupons. This implies that the strain concentration is diminished in close proximity to the hole boundary. The net stress based on ligament area at failure, 2543 MPa (368.8 ksi), agrees closely with the average static strength of the unnotched coupons, 2643 MPa (383.3 ksi).

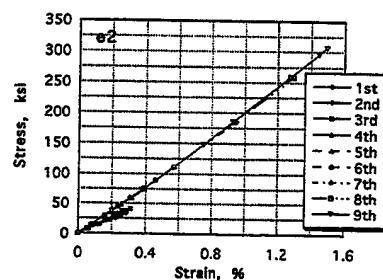


Figure 10. Experimental Strain Measurements from Gage e2 for Loadings 1-9.

In a similar fashion as the $[90_8]_T$ laminate, the experimental and theoretical strain results are compared in Figure 11. Results are shown for applied stresses of 102 MPa (14.8 ksi), 143 MPa (20.7 ksi), and 186 MPa (27 ksi). As expected SVELT slightly overpredicts the experimental strains; however, results agree within five percent for all cases. Note that the $[0_8]_T$ laminate produced a higher stress concentration compared to the $[90_8]_T$ laminate. Values of experimental strain concentration factors ranged from 5.92-9.2 at low loadings. Results are reported as 6.825 and 6.78 based on SVELT and Lekhnitskii's solution, respectively.

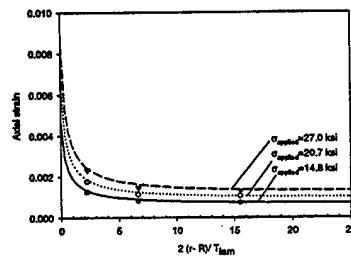


Figure 11. Comparison of Experimental and Theoretical Strains for $[0_\delta]_T$ Laminate.

2.2.4 $[\pm 45]_{2S}$ Laminate

The $[\pm 45]_{2S}$ laminate was tested for a series of six incremental loadings corresponding to the following values of applied stress: 51.07 MPa (7.410 ksi), 76.61 MPa (11.11 ksi), 86.83 MPa (12.59 ksi), 114.9 MPa (16.66 ksi), 140.5 MPa (20.38 ksi), and 158.3 MPa (22.96 ksi). On the sixth loading the laminate failed along the fiber direction similar to a typical unnotched $[\pm 45]_S$ tensile coupon. Figures 12a and 12b display radiographic images of the specimen following load steps 4 and 5, respectively, and Figures 13a through 13f show stress-strain curves for load steps 1 through 6. Note that the strain ϵ_1 is not shown after the third loading because of damage on the gage site.

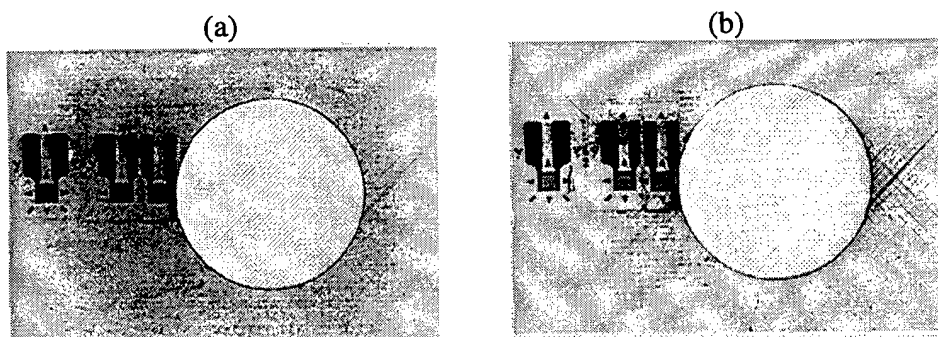


Figure 12. Radiographs of $[\pm 45]_{2S}$ Laminate for Stresses of (a) 114.9 MPa (16.66 ksi) and (b) 140.5 MPa (20.38 ksi).

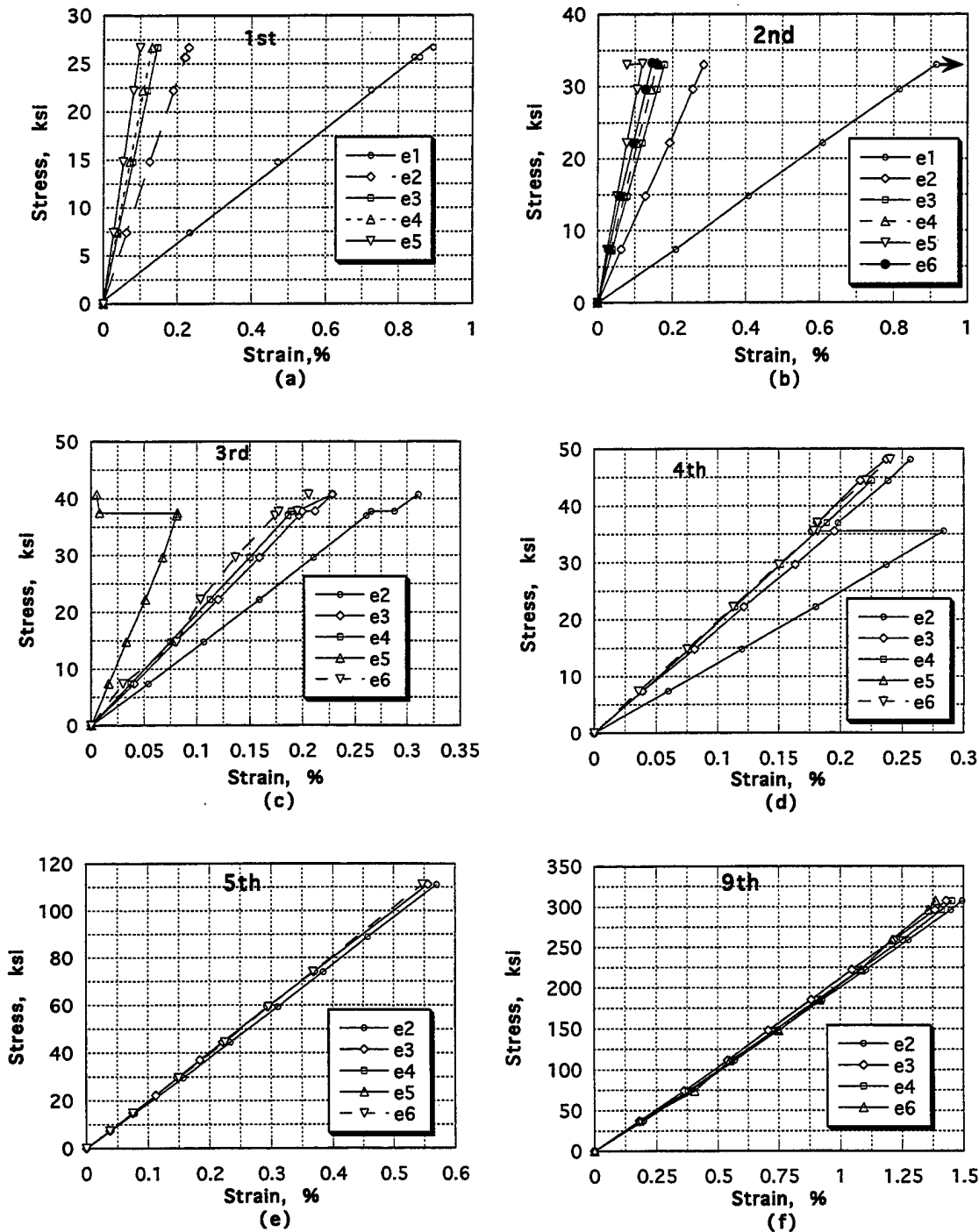


Figure 13. Stress-Strain Curves for Gages e1-e5 for $[\pm 45]_{28}$ Laminate at Load Steps: (a) 51.07 MPa (7.410 ksi), (b) 76.61 MPa (11.11 ksi), (c) 86.83 MPa (12.59 ksi), (d) 114.9 MPa (16.66 ksi), (e) 140.5 MPa (20.38 ksi), and (f) 158.3 MPa (22.96 ksi).

The onset of cracking as determined from radiographic images was observed after the fourth loading. Unlike the previous laminates, no single initial crack was identified. Rather, several transverse cracks in 45° and -45° plies were visible in Figure 12a, which describes the initial damage state after the fourth loading. Transverse cracks appear in close proximity to the strain gages originating approximately 75° clockwise from the reference direction in the 45° ply and 105° in the -45° ply. The longest crack appears in the -45° ply and emanates a distance 7.2 mm from the hole at 285° clockwise from the reference direction. The first significant acoustic emission event was recorded at 109.4 MPa (15.87 ksi), and further peaks continued until specimen unloading at 114.9 MPa (16.66 ksi). The cracks grew in succeeding loads, while multiple new cracks developed as shown in Figure 12b.

Upon examination of strain measurements in Figure 13, a decrease in strain ϵ_1 is evident between load steps 1, 2, and 3, until the strain behavior is almost exactly that of strain ϵ_2 for applied stresses below 96 MPa (14 ksi) in load step 4. This implies that stress relaxation occurred on the hole edge upon damage initiation. An increase of strain ϵ_2 at the sixth load demonstrates the effect of transverse crack growth on the stress-strain behavior. The far-field strain ϵ_5 remained unchanged until the fifth loading and increased by ~6 percent at the sixth loading, where transverse cracks occurred in the far-field region. This is demonstrated by a sudden change of stress-strain curve for ϵ_5 near the end of the fifth loading as shown in Figure 13e. Far-field strain ϵ_5 indicates some degree of damage at the fifth and sixth loadings. Note that all strains become highly nonlinear as stress level increases.

The net stress at failure was 205.5 MPa (29.80 ksi) and compared well with the unnotched tensile strength, 207.8 MPa (30.14 ksi). Good agreement between experimentally-measured strains and SVELT is shown in Figure 14 for applied stresses of 27.4 MPa (3.970 ksi),

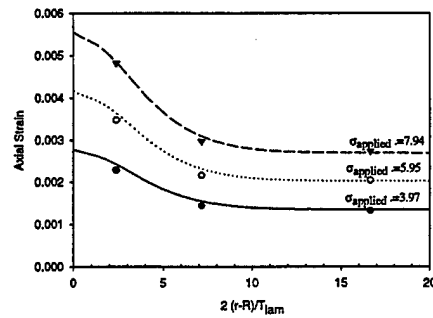


Figure 14. Experimental and Theoretical Strains for $[\pm 45]_{2S}$ Laminate.

41.0 MPa (5.950 ksi), and 54.7 MPa (7.930 ksi). The strain concentration factor was calculated in the initial linear region of stress-strain curves both experimentally and theoretically. The experimentally-determined average was 2.23 based on data from gage e1 and e5. Calculations from SVELT and Lekhnitskii resulted in values of 2.20 and 1.84, respectively.

3. CONCLUSIONS/RECOMMENDATIONS

- Method of superposition of a hybrid and displacement approximation was developed to provide accurate stress fields in the vicinity of the ply interface and the hole edge in a multilayered composite. The asymptotic analysis was used to derive the hybrid stress functions. The displacement approximation was based on polynomial B-spline functions.

- The multiplicative factor of the singular term in stress solution near the ply interfaces and the open hole edge was determined in $[45/-45]$ laminates under mechanical loading.

Convergence study showed that accurate values of the multiplicative factor of the singular term can be obtained with the coarse out-of-plane subdivision of one sublayer per ply. Converged transverse interlaminar stress components including the singular region were shown.

- Extension of this approach to thermal loading and fastener hole problems is among immediate future developments.

- An experimental investigation has been conducted on the initiation and growth of damage in close proximity to open hole $[0_8]_T$, $[90_8]_T$ and $[\pm 45]_{2S}$ laminates under incremental tension loading. The development of damage observed by x-ray radiography was correlated with the stress-strain behavior. Failure occurred without any prior evidence of damage for the $[90_8]_T$ laminate, whereas considerable damage was evident prior to failure of the $[0_8]_T$ and $[\pm 45]_{2S}$ laminates. As damage developed for the $[0_8]_T$ and $[\pm 45]_{2S}$ laminates, stress concentration decreased and the net stress at failure was nearly identical to the static strength of the respective unnotched coupon. However, for the $[90_8]_T$ laminate, the net stress at failure is related to the static strength of the unnotched specimen through a reduced stress concentration factor. For all laminates, the analytical predictions of strain concentration factors calculated by spline

variational theory and by elasticity showed good agreement with experimentally-measured results. Overall, a set of damage observations was developed for comparison with stress analysis methods that incorporate progressive damage modeling.

- Development of damage propagation modeling framework based on spline approximation stress analysis technique and correlation with the experimental results will be conducted.

4. PUBLICATIONS/PRESENTATIONS

Iarve, E. V. (1996). Three Dimensional Asymptotic and B-Spline Based Numerical Analysis of Composite Laminates with Fastener Holes. *Proceedings ASC 11th Technical Conference* (1086-1095).

Iarve, E. V. (1997). Three-Dimensional Stress Analysis in Laminated Composites with Fasteners Based on the B-Spline Approximation. *Composites Part A* 28A (559-571).

Iarve, E. V. (1997). Combined Asymptotic and B-Spline Based Approximation for 3-D Stress Analysis of Composite Laminates with Holes. *Proceedings of the 38th AIAA/ASME/ASCE/AHS/ASC Structures, Structural Dynamics and Materials Conference*.

Iarve, E. V. (1997, September). *Framework for Damage Initiation and Propagation Analysis for Composite Bolted Joints Based on Local Overlays of Spline Approximation Basis Functions*. Paper presented at Fourth SVELT Workshop, WPAFB, OH.

Iarve, E. V. (1997, June). *Overview of Spline Approximation Based Composite Bolted Joint Analysis Methods*. Paper presented at the Navy Research Laboratory, Washington, DC.

5. REFERENCES

1. Pagano, N. J. (1978). Stress Fields in Composite Laminates. *Int. J. Solids Structures* 14 (385-400).
2. Pagano, N. J. (1978). Free-Edge Stress Fields in Composite Laminates. *Int. J. Solids Structures* 14 (401-406).
3. Wang, S. S., & I. Choi. (1982). Boundary-Layer Effects in Composite Laminates: Part 1-Free-Edge Stress Singularities. *Journal of Applied Mechanics* 49 (541-548).
4. Wang, S. S., & I. Choi. (1982). Boundary-Layer Effects in Composite Laminates: Part 2-Free-Edge Stress Solutions and Basic Characteristics. *Journal of Applied Mechanics* 49 (549-560).
5. Tong, P., T. H. H. Pian, & S. J. Larsy. (1973). Hybrid-Element Approach to Crack Problems in Plane Elasticity. *Int. J. for Numerical Methods in Engineering* 7 (297-308).
6. Wang, S.S., & F. G. Yuan. (1983). A Hybrid Finite Element Approach to Composite Laminate Problems with Singularities. *Journal of Applied Mechanics* 50 (835-844).
7. Folias, E. S. (1992). On the Interlaminar Stresses of a Composite Plate Around the Neighborhood of a Hole. *Int. J. Solids Structures* 25 (1193-1200).
8. Wang, S.S., & X. Lu. (1993). Three-Dimensional Asymptotic Solutions for Interlaminar Stresses in Around Cutouts in Fiber Composite Laminates. In Y. D. S. Rajapakse, *Mechanics of Thick Composites* (AMD-Vol. 162, Book No. G00785, 41-50).
9. Iarve, E. V. (1996). Spline Variational Three Dimensional Stress Analysis of Laminated Composite Plates with Open Holes. *Int. J. Solids Structures* 44(14) (2095-2118).
10. Morley, L. S. D. (1969). A Modification of the Rayleigh-Ritz Method for Stress Concentration Problems in Elastostatics. *J. Mech. Phys. Solids* 17 (73-82).
11. Morley, L. S. D. (1970). A Finite Element Application of the Modified Rayleigh-Ritz Method. *Int. J. for Numerical Methods in Engineering* 2 (85-98).
12. Yamamoto, Yoshiyuki, & N. Tokuda. (1973). Determination of Stress Intensity Factors in Cracked Plates by the Finite Element Method. *Int. J. Numerical Methods in Engineering* 6 (427-439).
13. Yamamoto, Yoshiyuki, & Sumi Yoichi. (1978). Stress Intensity Factors for Three-Dimensional Cracks. *Int. J. of Fracture* 14 (17-38).

14. Shyprekevich, P. (1995). Characterization of Bolted Joint Behavior: MIL-HDBK-17 Accomplishments at Standardization. *Journal of Composites Technology & Research*, 17(3) (260-70).
15. Lekhnitskii, S. G. (1968). *Anisotropic Plates*. Gordon and Breach Science Publishers.
16. Garbo, S. P., & J. M. Ogonowski. (1981). *Effect of Variances and Manufacturing Tolerances on the Design Strength and Life of Mechanically Fastened Composite Joints*. AFWAL-TR-81-3041, Vols. I, II, and III. Dayton, OH: U.S. Air Force.
17. Snyder, B. D., J. G. Burns, & V. B. Venkayya. (1990). Composite Bolted Joints Analysis Programs. *Journal of Composites Technology & Research* 12(1) (41-51).
18. Iarve, E. V. (1995). *Three-Dimensional Stress Analysis of Fastener Hole Composites*. (AMD-Vol. 69-1, IMECE, American Society of Mechanical Engineering).
19. Shalev, D., & K. L. Reifsnider. (1990). Study of the Onset of Delamination at Holes in Composite Laminates. *Journal of Composite Materials* 24 (42-71).
20. Joshi, S. P., & Y. W. Huang. (1994). Damage Progression in the Vicinity of a Hole. *Journal of Thermoplastic Composite Materials* 7 (125-138).
21. Reddy, E. S., A. S. D. Wang, & Y. Zhong. (1990). Simulation of Matrix Cracks in Composite Laminates Containing a Small Hole. *Journal of Reinforced Plastics and Composites* 9 (104-117).
22. Lessard, L. B., & F. K. Chang. (1991). Damage Tolerance of Laminated Composites Containing an Open Hole and Subjected to Compressive Loading: Part II-Experiment. *Journal of Composite Materials* 25(1) (44-77).
23. Schaff, J. R., D. H. Mollenhauer, & D. H. Rose. (1996). Stress Analysis and Experimental Testing of a Structural Composite Laminate with a Hole. *Proceedings of the 11th American Society of Composites Technical Conference* (1049-58).